

Mask-guided cross-image attention for zero-shot *in-silico* histopathologic image generation with a diffusion model

Dominik Winter¹, Nicolas Triltsch¹, Marco Rosati¹, Anatoliy Shumilov¹, Ziya Kokaragac¹, Yuri Popov¹, Thomas Padel¹, Laura Sebastian Monasor¹, Ross Hill², Markus Schick¹, and Nicolas Brieu¹

¹ AstraZeneca Computational Pathology GmbH, Bernhard-Wicki-Str. 5. 80636 Munich, Germany

² AstraZeneca, Discovery Centre, 1 Francis Crick Avenue, Cambridge, CB2 0AA, United Kingdom

{Dominik.Winter,Nicolas.Brieu}@astrazeneca.com

Abstract. Creating *in-silico* data with generative AI promises a cost-effective alternative to staining, imaging, and annotating whole slide images in computational pathology. Diffusion models have become the state-of-the-art solution for generating *in-silico* images, offering unparalleled fidelity and realism. Using appearance transfer diffusion models furthermore allows for zero-shot image generation, facilitating fast application and making model training unnecessary. However current appearance transfer diffusion models are designed to work on natural images, where the main task is to transfer the foreground object from an origin to a target domain, while the background is of insignificant importance. In computational pathology it is however not straightforward to define which objects in an image should be classified as foreground and background, as all objects in an image may be of critical importance for the detailed understanding the tumor micro-environment. We contribute to the applicability of appearance transfer diffusion models to immunohistochemistry-stained images by modifying the appearance transfer guidance in the forward denoising process to alternate between class-specific AdaIN feature statistics matchings using existing segmentation masks. The performance of the proposed method is demonstrated on the downstream task of supervised epithelium segmentation, showing that the number of manual annotations required for model training can be reduced by 75% and outperforms the baseline approach. Additionally, we consulted with a certified pathologist to investigate future improvements. We anticipate this work to inspire the application of zero-shot diffusion models in computational pathology, providing an efficient method to generate *in-silico* images with unmatched fidelity and realism, which prove meaningful for downstream tasks, such as training existing deep learning models or finetuning foundation models.

Keywords: Diffusion models · Computational Pathology · Zero-shot

1 Introduction

Deep learning model development in computational pathology requires datasets that contain meaningful, relevant, and accurate information enabling models to learn to perform a desired task. This includes training models from scratch as well as for finetuning models such as foundation models to specific downstream tasks. Creation of meaningful datasets require multiple time-consuming steps in the wet lab as well as from computational side, including sample preparation, staining, imaging, digitalization, and multiple quality control steps. The curation of the Whole Slide Images (WSIs) datasets often not only requires a domain expert, but often also manual annotations of the images in a dataset. Manually annotating large sets of pathology images with pixel-level accuracy – as required for the training of supervised deep learning models, is a laborious and expensive task that binds precious resources. Synthetic data on the other hand is efficient and cheap to obtain, has controllable parameters, enabling the creation of exactly the data required. Recently, models trained on synthetic data have proven to learn better representations than models trained on real data [16]. In this work, we explore appearance transfer for generating *in-silico* data of immunohistochemistry (IHC) images in a zero-shot approach using a diffusion model. This approach can create realistic images with a fraction of the costs and effort as compared to creating real world datasets. We show that we can reduce the number of real-world images required to train a deep learning model to a fraction using our appearance transfer pipeline to generate *in-silico* images that match a segmentation mask with pixel-precise accuracy. To this end, we transfer the appearance of an existing image to an unpaired mask of morphological structures corresponding to a given spatial tissue and cellular spatial organization and thereby creating new images that resemble and expand the distribution of the images in the dataset. To enable the appearance transfer, we provide our appearance transfer model with an image and a corresponding mask of annotated epithelium. Then we provide another mask as well to which the image appearance will be transferred. Considering an image displaying regions of epithelium and stroma in each spatial organization, we seek to transfer the epithelium and stroma appearance into a different spatial organization, without mixing the two tissue types and while preserving their unique morphological characteristics.

1.1 Generative Models in Computational Pathology

In-silico image generation has a tremendous impact on computational pathology providing methods to create datasets of high realism and fidelity under controllable parameters alleviating costly and time-consuming manual work [4, 19]. CycleGANs provide an efficient way to generate *in-silico* data, they can be trained on unpaired images for tasks such as stain normalization [13], transfer learning [3] and data augmentation [17].

1.2 Diffusion Models in Computational Pathology

Diffusion models have recently emerged as a new state-of-the-art approach in biomedicine for *in-silico* image generation providing unmatched realism and fidelity as opposed to previous methods, such as CycleGANs. Conditional diffusion models enable to guide the diffusion models generative power to images with the desired properties. Thereby enabling to exactly steer the image generation towards datapoints most useful for downstream applications. Applications of diffusion models in medicine, biology and pathology [8, 14] span from segmentation [21], lesion detection [20], cell shape prediction [18], to artefact recovery [10]. In computational pathology diffusion models have been used to generate hematoxylin and eosin (H&E) stained images [10, 22] of rare cancer types that were indistinguishable from real images by pathologists. They have also been used for anomaly detection [9] and synthesis of nuclei segmentation and classification datasets [11, 15, 23] in H&E images. Text-conditioned diffusion models have been used to generate pathology H&E images using pathological reports [24]. Generating pixel-precise images poses a high requirement on the generative model, as opposed to for example generating images for a classification task, that requires only one label per image. It has been shown that diffusion models can be used in a multi-task setting for a pixel-precise H&E image to IHC image translation task, while simultaneously learning a H&E based cell segmentation [7]. Generating *in-silico* images at a gigapixel scale is also a unique challenge in computational pathology that can be solved with diffusion models [5] by adding fine details to images while increasing the images resolution with diffusion models or by preserving long-range correlation of structural information using segmentation masks to condition the diffusion model [2]. However, most of these models were developed on H&E images that are non-specific stains as opposed to IHC images which are directed to a specific protein marker. While H&E is the most used assay in histopathology, with hematoxylin highlighting the nucleus and eosin the cytoplasm of a cell, not all information required for a pathological assessment (*e.g.* disease grade or possible response to treatments) is displayed in H&E-stained images. IHC stains provide complementary information, as they can exactly show where specific proteins are located, highlighting different cell types, different cellular or tissue morphologies, allowing for an accurate pathological assessment. However, this further complicates *in-silico* data generation, as the diversity of IHC stained images is much higher and has a larger diversity and complexity than H&E images, potentially requiring new costly model development efforts for each new IHC assay. The discussed diffusion models require additional training, which generally require extensive and diverse datasets to converge, adding an impediment for their application, whereas zero-shot diffusion models enable fast data generation pipelines, not restricted by any specific assay or indication. Our model on the other hand does not require additional dataset-specific training, making it ideal for zero-shot applications, thus making it easy and fast to apply and saving precious resources typically required for model development.

1.3 Diffusion Models for Appearance Transfer

Denoising Diffusion Probabilistic Models (DDPMs) can generate images from gaussian noise. They are trained by successively adding noise to an image to obtain noisy samples, a process that can be described by a Markov Chain. The reverse denoising process is learned by the model. During inference the denoising process is repeated numerous times to generate an image from gaussian noise. Recent work shows that cross- and self-attention mechanisms in DDPMs can encode semantic information and by mixing the keys, queries and values in the transformer layers of the denoising model with a cross-attention mechanisms appearance transfer between images can be achieved [1]. For each forward pass through the network during the denoising diffusion process the keys, values and queries are projected through the learned linear projections in each self-attention layer of the network. The attention score, indicating how relevant each key is for the corresponding query, is then calculated for all keys and weighted by a SoftMax operation before they are aggregated to an attention map that enables capturing of correspondences across the entire image. Alaluf et al. have showed that semantic information contained in the queries, keys, and values captured by the self-attention layers can be used to transfer information between images. While the queries capture the semantic information of each spatial location, the keys offer context for the queries and the values contain the content that is transferred from the origin image to the target structure. As opposed to the appearance transfer of natural images where foreground transfer of the foreground object (*e.g.* an animal) is the main interest and the background (*e.g.* the sky) is of minor importance, in pathological images foreground and background cannot be easily selected, as individual classes (for example epithelium and stroma) are of similar importance and their realism are equally decisive in downstream tasks.

1.4 Our Contribution

We have developed a novel generative Artificial Intelligence approach to create meaningful *in-silico* histopathology images. Using appearance transfer we can provide the model with an image containing the desired style of the generated pathology image and a segmentation mask, containing the desired structure of the generated images. Our contributions comprise:

- We modify an existing generative diffusion model pipeline by replacing a segmentation-based feature statistics mask guidance by a class specific mask guidance to allow for appearance transfer from an IHC image to a segmentation mask. This required the following adaptations of Alaluf et al.s generative pipeline. We use existing segmentation masks from the origin m_{origin} and target domain m_{target} to guide the appearance transfer through the AdaIN feature statistics matching mechanism of the pipeline, as opposed to relying on a self-supervised segmentation model that segments only the foreground area during the AdaIN operation.

- We modify the forward denoising process to alternate between the feature statistics masked with the class-specific mask in each forward denoising step to ensure all classes in an image are generated with equally well transferred feature statistics.
- We show that our approach outperforms the baseline approach, proving that we can improve the visual realism of the generated images noticeable, especially for the class that was previously detected as background.
- We provide evaluation assessing the benefit for a downstream epithelium semantic segmentation task that achieves similar model performance when trained only with 25% of a fully annotated training dataset using additional *in-silico* data generated with our diffusion model as compared to another model trained on the full dataset without *in-silico* data.

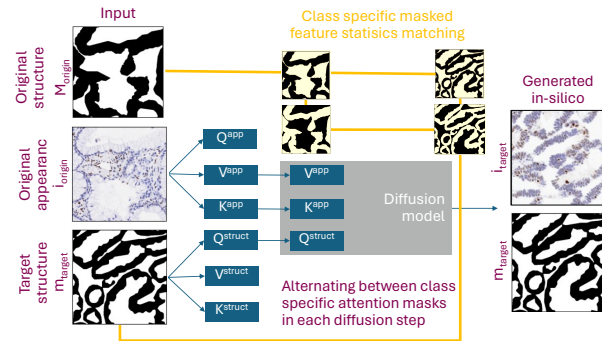


Fig. 1: Zero-shot appearance transfer from an IHC images to a target structure enabled by diffusion models. By swapping the values and keys from the origin appearance image (i_{origin}) with the queries from the target structure image (m_{target}) we can transfer the appearance to the structure generating new *in-silico* images (i_{target}). Class specific masked feature statistics matching during the AdaIN operation between the structure and appearance guides the diffusion process alternating between the classes contained in the mask.

2 Methods

2.1 Zero-shot *in-silico* Image Generation Pipeline

We utilize a diffusion model as a state-of-the art approach in generative AI to transfer IHC images from an origin domain to a target domain. Inspired by Alaluf et al.’s model [1] to perform an appearance transfer from existing IHC images to masks through classifier-free guidance. We aim to generate *in-silico* images with realistic IHC appearance and a matching segmentation mask which is pixel-precise, so that the generated image and mask can be used to train

semantic segmentation models. Our model requires a pair of an image i_{origin} and corresponding segmentation mask m_{origin} from the origin domain and a mask m_{target} of the target domain to which a corresponding *in-silico* image i_{target} is generated. Through controlling the structure in m_{target} we ensure the generated image i_{target} is a morphologically realistic and meaningful representative of a dataset.

2.2 Multi-Class Guided Diffusion Model

For a pair of images, one containing an IHC image i_{origin} (*e.g.* NSCLC tissue showing nuclei with either negative hematoxylin or positive DAB staining) and one contain its pixel-precise segmentation mask i_{origin} and one contain its pixel-precises segmentation mask m_{origin} we aim to transfer the appearance of an image i_{origin} to a new structure m_{target} , generating the *in-silico* image i_{target} (see Fig. 1). Inspired by Alaluf et al.’s approach we use Stable Diffusion [12] as a pretrained text-to-image model to perform the zero-shot appearance transfer. (see Fig. 1). Inspired by Alaluf et al.’s approach [1] we use Stable Diffusion [12] as a pretrained text-to-image model to perform the zero-shot appearance transfer. By replacing the keys and values of the image i_{origin} image and preserving the queries from the mask m_{target} a transfer of the appearance contained in i_{origin} to the structure of m_{target} between semantically similar objects is enabled. We modify this appearance transfer mechanism by employing a class specific feature statistics matching in the AdaIN operation to be guided by the existing segmentation mask m_{origin} and m_{target} through the class-specific masked latents.

2.3 Mapping Classes to Timesteps

As a first step of the appearance transfer the inverted latents $z_T^{i_{origin}}$ and $z_T^{m_{target}}$ are calculated. At each forward step t we pass the latents to the denoising U-Net. In the decoder of the U-Net the standard self-attention was replaced with the cross-image attention as suggested by Alaluf et al. [1]. Secondly, we map the number of classes to the timesteps in an alternating fashion that allows for alternating between class-specific masking of the AdaIN operation for every forward step t in the denoising process. For each denoising step t two forward steps through the network are performed, the first using the cross-attention layer:

$$\epsilon^{cross} = \epsilon_{\theta}^{cross}(z_t^{out}) \quad (1)$$

and the second using the self-attention layer of the network:

$$\epsilon^{self} = \epsilon^{self}(z_t^{out}) \quad (2)$$

The two noise predictions are then aggregated:

$$\epsilon^t = \epsilon^{self} + \alpha(\epsilon^{cross} - \epsilon^{self}) \quad (3)$$

While α denotes the guidance scale, z_{t-1}^{out} is the latent code at $t - 1$ and ϵ^t is the modified noise. We found this enhances the fidelity and realism of the

class that the model identified as background in original implementation. In the example of a two-class appearance transfer in every even denoising step the mask of the first class would be used and in every uneven denoising step the mask of the second class.

2.4 Feature Statistics Matching with Masked AdaIN

We use the AdaIN operation to match feature statistics between the latent representations as Alaluf et al. [1]. Because we desire to match feature statistics of the class specific regions exclusively with feature of the same class regions, we utilize the binary masks m_{origin} and m_{target} to mask the foreground or background respectively. Therefore, we alternate between the binary masks that guide the feature statistics matching in the AdaIN operation between the masks that denote the respective class in each denoising step. For c being the class, we apply a mask over the latents $z_{t,c}^{i_{origin}} = mask(z_t^{i_{origin}})$ and $z_{t,c}^{m_{target}} = mask(z_t^{m_{target}})$ to restrict the AdaIN operation on this class specific mask. Then we apply the AdaIN operation $z_{t,c}^{out} = AdaIN(z_{t,c}^{m_{target}}, z_{t,c}^{i_{origin}})$ to align the color distributions of each class between the generated image and the input image. In the example of a two-class task, the AdaIN operation is masked with binary masks that describe the first class in even denoising steps t and the second class (which is the inverse binary mask) in uneven denoising steps t .

3 Experiments

3.1 Data Generation

Due to the probabilistic nature of diffusion models, we can create infinitely new variants of each image in a dataset where every generated image varies from the others. During the image generation process we have observed that our diffusion model performs best when the classes between the origin and target image contain similar numbers of pixels and mask shapes. Therefore, we select masks from the same dataset with similar class distributions as target structures for a given image of the origin domain. By selecting masks from the same dataset, as opposed to generating new masks we ensure our masks contain morphologically sensible structures. To increase the diversity of the generated images we augment the target masks with spatial augmentations, such as flips and rotations. For the denoising process, we use the standard DDIM scheduler for 100 denoising steps. As introduced by Alaluf et al. we inject the keys and values only at timesteps between 10 and 70 for layers with a resolution of 32x32 and for timesteps between 10 and 90 for layers at resolution 64x64 and apply the AdaIN operation at timesteps between 20 and 100 [1].

3.2 Data Pre-processing

For the input image i_{origin} the pixel values are given, however for the target mask m_{target} there are arbitrary possibilities to set the pixel values describing the pixel

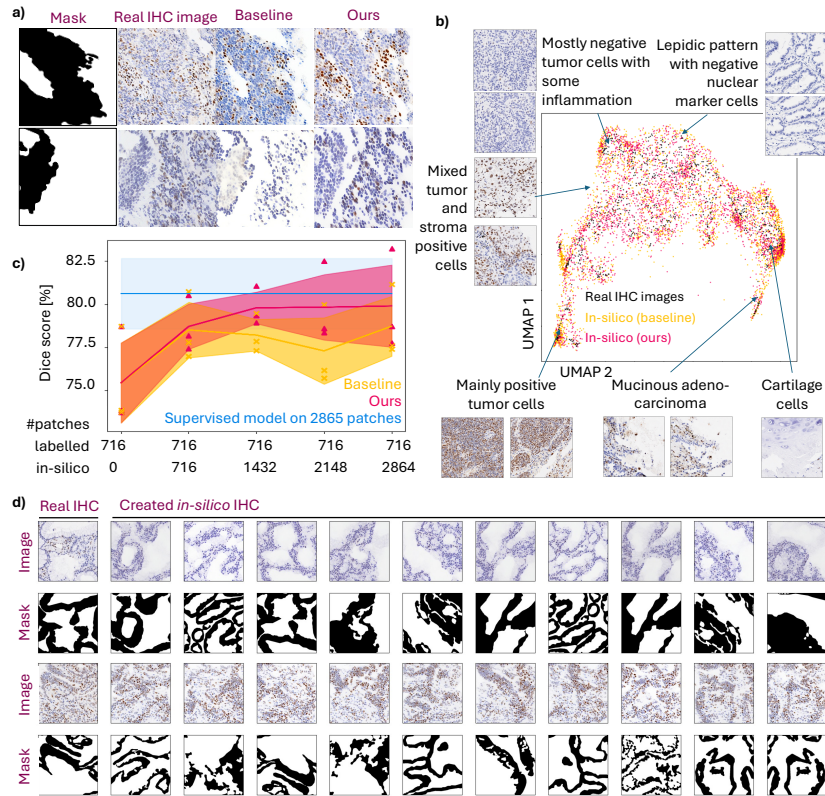


Fig. 2: Our zero-shot image generation pipeline generates realistic IHC images that allow for a reduction of 75% of manual annotations. **a** Our model visually outperforms the baseline (out-of-the-box) model yielding images with more realistic morphological structures, especially in the class detected as background by the baseline model. Mask and original image are displayed for reference, for comparability the same structure was used for all images **b** Encoding each image embedding, obtained by encoding each image with a ViT into a two-dimensional space using UMAP, we find overlapping distributions between the real IHC images and the *in-silico* images of the baseline and our model. **c** From a dataset of 2864 manually annotated images, we use a subset of 25% (716) images and recreate one to four *in-silico* images for each image, adding them step-wise and train each time a new model comprising of partially real and *in-silico* data. Semantic epithelium segmentation models deliver the best performance using images generated with our appearance transfer diffusion model (red), outperforming the baseline model (yellow), reaching the performance of a model trained on all manually annotated images (blue). Our test-set was annotated by 3 independent pathologists, Dice scores (triangles), the mean (solid line) and standard deviation (colored area) are displayed. **d** With our diffusion model infinitely many new versions of a real image can be generated, here 9 *in-silico* images with the same appearance but different structures are shown.

areas of the classes in each image. Naively one would set integers as class values, however from experiments, we realized that setting the mask pixel values to 0.1 and 0.5 for the two classes in our experiments provided visually the best results, while adding a tiny amount of gaussian noise (variance: 0.0001) further improved the realism of the images. We found that adding a larger amount of gaussian noise saturated the colors for our generated images. To guide the appearance transfer, we utilize masked feature statistics matching in the AdaIN operation using binary masks with pixel values of 0 and 1, which we invert, dependent on which class we wanted to guide the appearance transfer (see Fig. 1).

3.3 Semantic Segmentation Model Training

The selected models were tested on a held-out test set containing images of Non-Small Cell Lung cancer stained with a nuclear marker (*e.g.* Ki67), split on patient level and containing manual annotations from one or three pathologists in selected FOVs. For our experiment we utilize a U-Net model with an EfficientNetV2S backbone. We trained models optimizing the combined binary cross entropy and dice loss. All models were trained using the ADAM optimizer, with a learning rate of 0.001, beta1 of 0.9 and beta2 of 0.99 and using early stopping. The best model was selected based on the validation set that was split from the dataset on a WSI level. For all model trainings the same set augmentations were used, comprising spatial augmentations such as shifts, rotations, flips and shears as well as color augmentations such as blurs (gaussian & motion), brightness, contrast, gamma, hue and saturation augmentations.

3.4 Evaluation of Semantic Segmentation Models

The segmentation model’s performance was calculated using annotation of 3 pathologists on a held-out test-set calculating the Dice score on a FOV level and aggregating the scores for all FOVs.

4 Results

In a quiver of experiments, we showcase the utility of the generated *in-silico* images, for example in training supervised semantic models and explore applications in the field of computational pathology displaying potential applications of our generative AI model. This includes epithelium segmentation in immunohistochemistry (IHC) images with a semantic segmentation model.

4.1 Utility of *in-silico* Images in Supervised Semantic Segmentation Model Development

In a **first experiment** we investigate the utility of the generated *in-silico* data. Our downstream application is a semantic epithelium segmentation task, as a representative task in computational pathology. The dataset used to prove the

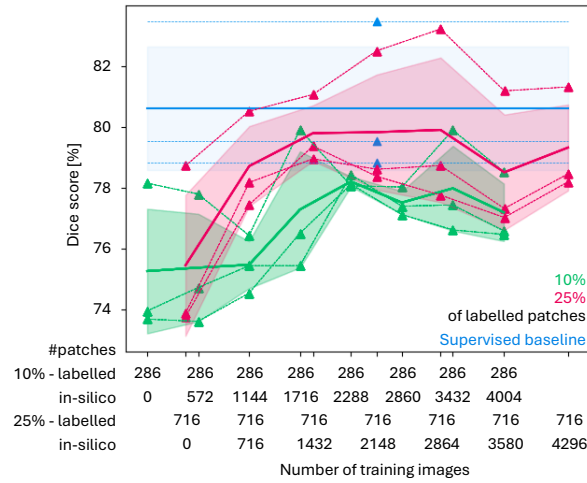


Fig. 3: Multiple folds of generated *in-silico* images prove useful for downstream model training, but performance increases saturated. For subsets (10% equaling 286 patches and 25% equaling 716 patches of the original annotated training dataset), we train semantic epithelium segmentation models on the original images and then iteratively add rounds of generated *in-silico* images to the training. The performance of the semantic epithelium segmentation models saturates after five rounds (equaling 3580 generated *in-silico* images) in the 25% data regime and after eight rounds (equaling 2288 generated *in-silico* images) in the 10% data regime. The x-axis displays the total number of images (real plus *in-silico*) in the training set used for each training run of the semantic epithelium segmentation model. Our test set was annotated by 3 independent pathologists. Respective Dice scores of the segmented epithelium regions against each pathologist (triangle, dotted lines) are displayed together with the corresponding mean (solid line) and standard deviation.

utility of *in-silico* images in supervised model training comprises a training set of 61 WSIs of Non-Small Cell Lung Cancer (NSCLC) resections, stained with a nuclear marker assay, imaged with an Aperio AT2 scanner in 20x resolution. In these WSIs 163 Field-of-Views (FOVs) were placed and epithelium regions were annotated by one pathologist. This resulted in 2865 annotated patches (512x512px) in the training set and 1203 annotated patches in a validation set, split on a WSI level. An independent test-set was created from biopsies stained with the same nuclear marker assay (*e.g.* Ki67) and imaged with an Aperio AT2 scanner of NSCLC patients. Three independent pathologists annotated epithelium regions in 39 FOVs distributed across 18 WSIs. For our experiments, we subsampled the training and validation set to 10% and 25% respectively and used the diffusion models to generate new versions of each image in the training set (see Fig. 2, Fig. 3). For each round of generated *in-silico* images, we train semantic segmentation models from scratch and evaluated them on our test

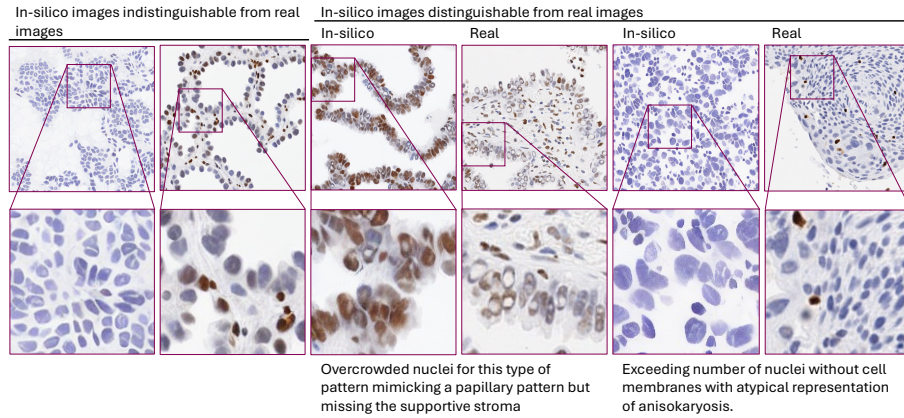


Fig. 4: Images generated with our zero-shot appearance transfer pipeline show convincingly realistic morphologies in many cases, improvements in selected morphological details are possible. We consulted with a board-certified pathologist to assess the differences between real and *in-silico* images. Despite the diffusion model being trained on images from animal tissues, some generated *in-silico* IHC images were indistinguishable from real images in the assessment process by the pathologist (two columns on the left). In some images the pathologist pointed us to cells displaying areas of future improvements, namely selected nuclear patterns (columns on the right), real images of similar morphologies are displayed for comparison.

set to measure the performance against the annotations of three independent pathologists.

Results show that we can reduce the number of pathology annotations by 75% and can reproduce each image in the training set four times without compromising model performance. We obtained a dice score of $(80.60\% \pm 2.04\%)$; mean \pm standard deviation) for the model trained on all 2865 patches annotated and a dice score of $(79.90\% \pm 2.37\%)$ for the model trained on 25% of the annotated patches (716 patches) and five rounds of *in-silico* images (2864 patches), i.e. a decrease of only 0.86% compared to the use of all patches. In comparison, the model trained only on 25% (716 patches) of the dataset, without using the generated *in-silico* data obtained a dice score of $(75.44\% \pm 2.32\%)$, i.e. a decrease of 6.4% compared to the use of all training patches and of 5.6% compared to the use of the same reduced amount of training patches and the proposed *in-silico* data generation. Similarly, reducing the dataset to 10% only (286 patches) yields a model reaching a dice score of $(75.44\% \pm 2.04\%)$, which we improved to a dice score of $(78.20\% \pm 0.16\%)$ by adding *in-silico* data generated with our diffusion model to the training dataset (see Fig. 3). Our model yields an improvement over the baseline (out-of-the-box model) $(78.72\% \pm 1.73\%)$ where the performance saturates after one round of *in-silico* data generation, while the data generated with our model allows for further performance increases (see Fig. 2c). Using an encoder (ViT) model trained in a self-supervised manner [6].

on IHC images, we encode feature vectors of the images in the training dataset and the generated *in-silico* images from both the baseline model and our model and observe that both models are creating images that fall in similar distributions after reducing the feature vectors to 2D using a UMAP (see Fig. 2b). We furthermore investigated how many rounds of augmentation with the diffusion model are beneficial and we find that on a dataset reduced to 10% of the original dataset size, the segmentation model’s performance saturates after eight rounds of added *in-silico* (e.g. adding eight replicates of *in-silico* images for each image in the training dataset) with the diffusion model (see Fig. 3) and for the 25% dataset it saturates after five rounds of added *in-silico* data.

4.2 Realism Assessment with a Board-Certified Pathologist

In a **second experiment** we examine the realism of the IHC images created by the diffusion model with a board-certified pathologist to investigate limitations and areas of improvement on the same dataset as used for the first experiment. While most of the morphologies still seemed realistic as compared between the real and *in-silico* images for the pathologist, some differences were found (see Fig. 4). These differences were mainly found in overcrowded nuclear regions that displayed unrealistic morphologies for NSCLC mimicking a papillary pattern but missing the supportive stroma, and in regions with exceedingly high nuclear density without corresponding cell membranes accompanied by atypical representation of nuclear size and shape variation (anisokaryosis).

4.3 Discussion

In this study we present a novel diffusion model-based data generation pipeline, adapted to the requirements of computational pathology. Bypassing model training we show how the existing pipeline, trained on images of animals, can be used in a zero-shot fashion in computational pathology. We extend Alaluf et al.’s zero-shot appearance transfer pipeline developed for natural images by replacing a segmentation-based feature statistics mask guidance by a class specific mask guidance to allow for appearance transfer from an IHC image to a segmentation mask and thereby guide the appearance transfer through the AdaIN feature statistics matching mechanism. Furthermore, we modify the forward denoising process to alternate between the feature statistics masked with the class-specific mask in each forward denoising step to ensure all classes in an image are generated with equally well transferred feature statistics. Thereby we can generate more realistic IHC images that outperform the out-of-the-box pipeline on the downstream task of semantic epithelium segmentation. We showcase the utility of the generated images in downstream semantic segmentation model development tasks. Therefore, we generate *in-silico* images and segmentation masks, with pixel-precise matches between images and masks. The utility of the generated *in-silico* images is proven in downstream tasks, where the *in-silico* images facilitate a supervised model to reach performances previously only attainable with costly manual annotations. Using this pipeline, we show that pathology

annotations required for semantic segmentation model training can be reduced by roughly 75% without compromising model performance. In an extension to this first experiment, we investigated to which extent we can use the probabilistic nature of the diffusion models to generate multiple new versions of the same image with similar appearance but different structure, finding that initial improvements are substantial but saturate after multiple rounds. This can be explained by the limited information contained in the real dataset that is then expanded with our diffusion model. Additionally, we find that although *in-silico* data proves an efficient and cheap way to boost model performance, models trained on the same number of real images still perform better. With a certified pathologist we investigate the limitations of our data generation approach on another dataset with membrane IHC marker, discovering that the main differences between real and *in-silico* images are visible within some nuclei in the image, mainly found in the nuclear morphology. We find this an expected result, as our model weights were trained on an animal domain, thus not allowing the model to have learned any cellular morphologies, raising the question if future investments should go towards development of a foundation model for zero-shot appearance transfer specialized for microscopy images. We acknowledge that our approach is not applicable in a fully unsupervised setup that contains no annotations at all, because a corresponding segmentation mask is required from the origin domain to guide the appearance transfer. Furthermore, it remains yet to be explored how our model performs in cases where more than two classes are present in one image. In conclusion, we believe that this work contributes to the application of generative models in computational pathology and related fields, showing how zero-shot models can be employed in a resource efficient way to generate meaningful *in-silico* data across IHC assays that benefits downstream tasks. In future we plan to use our generative diffusion model pipeline on other IHC assays and indications.

References

1. Alaluf, Y., Garibi, D., Patashnik, O., Averbuch-Elor, H., Cohen-Or, D.: Cross-image attention for zero-shot appearance transfer. arXiv preprint arXiv:2311.03335 (2023)
2. Aversa, M., Nobis, G., Hägele, M., Standvoss, K., Chirica, M., Murray-Smith, R., Alaa, A.M., Ruff, L., Ivanova, D., Samek, W., et al.: Diffinfinite: Large mask-image synthesis via parallel random patch diffusion in histopathology. *Advances in Neural Information Processing Systems* **36** (2024)
3. Brieu, N., Meier, A., Kapil, A., Schoenmeyer, R., Gavriel, C.G., Caie, P.D., Schmidt, G.: Domain adaptation-based augmentation for weakly supervised nuclei detection. COMPAY workshop - arXiv preprint arXiv:1907.04681 (2019)
4. Brieu, N., Triltsch, N., Wortmann, P., Winter, D., Saran, S., Rebelatto, M., Schmidt, G.: Auxiliary cyclegan-guidance for task-aware domain translation from duplex to monoplex ihc images. arXiv preprint arXiv:2403.07389 (2024)
5. Harb, R., Pock, T., Müller, H.: Diffusion-based generation of histopathological whole slide images at a gigapixel scale. In: *Proceedings of the IEEE/CVF Winter Conference on Applications of Computer Vision*. pp. 5131–5140 (2024)

6. He, K., Chen, X., Xie, S., Li, Y., Dollár, P., Girshick, R.: Masked autoencoders are scalable vision learners. In: Proceedings of the IEEE/CVF conference on computer vision and pattern recognition. pp. 16000–16009 (2022)
7. Kataria, T., Knudsen, B., Elhabian, S.Y.: Staindiffuser: Multitask dual diffusion model for virtual staining. arXiv preprint arXiv:2403.11340 (2024)
8. Kazerouni, A., Aghdam, E.K., Heidari, M., Azad, R., Fayyaz, M., Hacihaliloglu, I., Merhof, D.: Diffusion models in medical imaging: A comprehensive survey. *Medical Image Analysis* p. 102846 (2023)
9. Linmans, J., Raya, G., van der Laak, J., Litjens, G.: Diffusion models for out-of-distribution detection in digital pathology. *Medical Image Analysis* **93**, 103088 (2024)
10. Moghadam, P.A., Van Dalen, S., Martin, K.C., Lennerz, J., Yip, S., Farahani, H., Bashashati, A.: A morphology focused diffusion probabilistic model for synthesis of histopathology images. In: Proceedings of the IEEE/CVF winter conference on applications of computer vision. pp. 2000–2009 (2023)
11. Oh, H.J., Jeong, W.K.: Diffmix: Diffusion model-based data synthesis for nuclei segmentation and classification in imbalanced pathology image datasets. In: International Conference on Medical Image Computing and Computer-Assisted Intervention. pp. 337–345. Springer (2023)
12. Rombach, R., Blattmann, A., Lorenz, D., Esser, P., Ommer, B.: High-resolution image synthesis with latent diffusion models. In: Proceedings of the IEEE/CVF conference on computer vision and pattern recognition. pp. 10684–10695 (2022)
13. Shaban, M.T., Baur, C., Navab, N., Albarqouni, S.: Staingan: Stain style transfer for digital histological images. In: ISBI. pp. 953–956. IEEE (2019)
14. Shokrollahi, Y., Yarmohammadtoosky, S., Nikahd, M.M., Dong, P., Li, X., Gu, L.: A comprehensive review of generative ai in healthcare. arXiv preprint arXiv:2310.00795 (2023)
15. Shrivastava, A., Fletcher, P.T.: Nasdm: nuclei-aware semantic histopathology image generation using diffusion models. In: International Conference on Medical Image Computing and Computer-Assisted Intervention. pp. 786–796. Springer (2023)
16. Tian, Y., Fan, L., Chen, K., Katabi, D., Krishnan, D., Isola, P.: Learning vision from models rivals learning vision from data. arXiv preprint arXiv:2312.17742 (2023)
17. Wagner, S.J., Khalili, N., Sharma, R., Boxberg, M., Marr, C., de Back, W., Peng, T.: Structure-preserving multi-domain stain color augmentation using style-transfer with disentangled representations. In: Medical Image Computing and Computer Assisted Intervention–MICCAI 2021: 24th International Conference, Strasbourg, France, September 27–October 1, 2021, Proceedings, Part VIII 24. pp. 257–266. Springer (2021)
18. Waibel, D.J., Röell, E., Rieck, B., Giryes, R., Marr, C.: A diffusion model predicts 3d shapes from 2d microscopy images. In: 2023 IEEE 20th International Symposium on Biomedical Imaging (ISBI). pp. 1–5. IEEE (2023)
19. Winter, D., Triltsch, N., Plewa, P., Rosati, M., Padel, T., Hill, R., Schick, M., Brieu, N.: Restaingan: Leveraging ihc to if stain domain translation for in-silico data generation. arXiv preprint arXiv:2403.06545 (2024)
20. Wolleb, J., Bieder, F., Sandkühler, R., Cattin, P.C.: Diffusion models for medical anomaly detection. In: International Conference on Medical image computing and computer-assisted intervention. pp. 35–45. Springer (2022)
21. Wolleb, J., Sandkühler, R., Bieder, F., Valmaggia, P., Cattin, P.C.: Diffusion models for implicit image segmentation ensembles. In: International Conference on Medical Imaging with Deep Learning. pp. 1336–1348. PMLR (2022)

22. Xu, X., Kapse, S., Gupta, R., Prasanna, P.: Vit-dae: Transformer-driven diffusion autoencoder for histopathology image analysis. In: International Conference on Medical Image Computing and Computer-Assisted Intervention. pp. 66–76. Springer (2023)
23. Ye, J., Ni, H., Jin, P., Huang, S.X., Xue, Y.: Synthetic augmentation with large-scale unconditional pre-training. In: International Conference on Medical Image Computing and Computer-Assisted Intervention. pp. 754–764. Springer (2023)
24. Yellapragada, S., Graikos, A., Prasanna, P., Kurc, T., Saltz, J., Samaras, D.: Pathldm: Text conditioned latent diffusion model for histopathology. In: Proceedings of the IEEE/CVF Winter Conference on Applications of Computer Vision. pp. 5182–5191 (2024)